Structures of N_2Ar, O_2Ar, and O_2Xe dimers studied by Coulomb explosion imaging

J. Wu,[1,2] M. Kunitski,[1] L. Ph. H. Schmidt,[1] T. Jahnke,[1] and R. Dörner[1,a)]
[1]*Institut für Kernphysik, Goethe-Universität, Max-von-Laue-Strasse 1, D-60438 Frankfurt, Germany*
[2]*State Key Laboratory of Precision Spectroscopy, East China Normal University, Shanghai 200062, China*

We use intense femtosecond laser pulses to multiply ionize and directly image the structures of N_2Ar, O_2Ar, and O_2Xe dimers by coincidently measuring the momenta of the fragment ions. All these dimers are found to have an equilibrium T-shaped structure in which the bond of the diatomic molecule is perpendicular to the dimer axis. The equilibrium distance between the rare-gas atom and the center-of-mass of the diatomic molecule is estimated to be $R_{N2-Ar} \sim 3.86$ Å, $R_{O2-Ar} \sim 3.65$ Å, and $R_{O2-Xe} \sim 4.07$ Å, respectively. For the T-shaped N_2Ar dimer, both sequential and direct triple-ionization-induced three-body breakups are observed. In contrast to N_2Ar dimer, other structures are found to coexist with the dominating T-shaped one for O_2Ar and O_2Xe. © *2012 American Institute of Physics*. [http://dx.doi.org/10.1063/1.4750980]

Molecules and atoms can bind with each other via the van der Waals force to form dimers. Such mixed species between a rare-gas atom and a diatomic molecule are highly interesting as they contain two bonds of very different characters: a very long and weak van der Waals bond between the rare-gas atom and the molecule and a covalent bond of a diatomic molecule. The most simple of these systems N_2Ar,[1–6] O_2Ar,[7–9] and O_2Xe[10–12] have been observed for about 40 yr. The previous experimental measurements[1,2,7,8,10–12] and theoretical calculations[3–5] indicate that the T-shaped geometry represents the ground state structure of these dimers. However, to the best of our knowledge, no direct observation of this T-shaped structure has been reported so far. Here, we directly image the structure of the dimer by Coulomb exploding it with intense femtosecond laser pulse. This is accomplished by means of a coincident measurement of the momenta of the fragment ions from the triple-ionization-induced three-body breakup. All these molecule-atom dimers are visualized to have a T-shaped structure. In contrast to N_2Ar, additional structures are found to coexist with the dominating T-shaped one in O_2Ar and O_2Xe.

The Coulomb explosion imaging[13] is a powerful tool to visualize the structures of polyatomic molecules[14–20] and van der Waals-force bound complexes.[21] After sudden stripping off several electrons by fast traversal through a thin foil,[13] or by multiple ionization with ion impact[14] or high-energy photon[15] or intense ultrashort laser pulse,[16–21] the multiply charged molecular ion typically fragments along the Coulomb potential curve. The relative momenta of the mutually repelling fragment ions hence reveal the initial structure of the molecule prior to the fast breakup. The latest of these experiments with this technique even resolve the nodes of the vibrational structure.[22]

We performed our measurements in a reaction microscope of cold target recoil ion momentum spectroscopy (COLTRIMS).[23,24] The dimers were generated by co-expanding the mixture of molecules (N_2 or O_2) and atoms (Ar or Xe) through a 30 μm nozzle with a driving pressure of 3.5 bars. The gas ratios in the mixture were N_2:Ar $\sim$ 1:1, O_2:Ar $\sim$ 1:7, and O_2:Xe $\sim$ 1:1 for the generation of N_2Ar, O_2Ar, and O_2Xe dimers, respectively. In the supersonic expansion the gas cools. In our jet also pure Ar_2 is formed. The Coulomb explosion image of Ar_2 from our nozzle expansion is compared to the wave function of the vibrational ground state of Ar_2, see Fig. 2(a) in Ref. 21, and there is no visible contribution of vibrationally excited states of the Ar_2 in our jet. The vibrational spacing in the ground state of Ar_2 is 3.2 meV. We therefore expect that also our mixed dimers are internally significantly colder than 3.2 meV. The femtosecond laser pulse with 35 fs duration centered at 790 nm produced from a Ti:Sapphire laser system was focused by a concave mirror ($f = 7.5$ cm) onto the gas jet inside the chamber. The laser intensities were measured to be $I_0 \sim 1.2 \times 10^{15}$ W/cm^2 for N_2Ar, and $I_0 \sim 6.0 \times 10^{14}$ W/cm^2 for O_2Ar and O_2Xe, respectively, where the laser intensity sensitive branching ratios of H$^+$ spectrum from the dissociation channel of H_2^+[25] were used for the calibration. The ions created by photo-ionization were accelerated with a weak ($\sim$14.7 V/cm) static electric field and detected by a time and position sensitive micro-channel plate detector[26] at the end of the spectrometer. The 3D momenta and kinetic-energy release (KER) of the fragment ions were calculated during the offline data analysis.

We distinguish the three-body breakup of the dimer from the random coincidences between ions originating from different atom or molecules ionized independently but by the same laser pulse by requiring the sum-momentum of the detected three particles, $p_{sum} = |p_1 + p_2 + p_3|$, to be less than 15 a.u. to account for the momentum conservation, and simultaneously the KER of Ar$^+$ (or Xe$^+$) being greater than 0.3 eV to make sure that Ar$^+$ (or Xe$^+$) is not from the single ionization of the atomic monomer, and the total KER of the

a)Electronic mail: doerner@atom.uni-frankfurt.de.
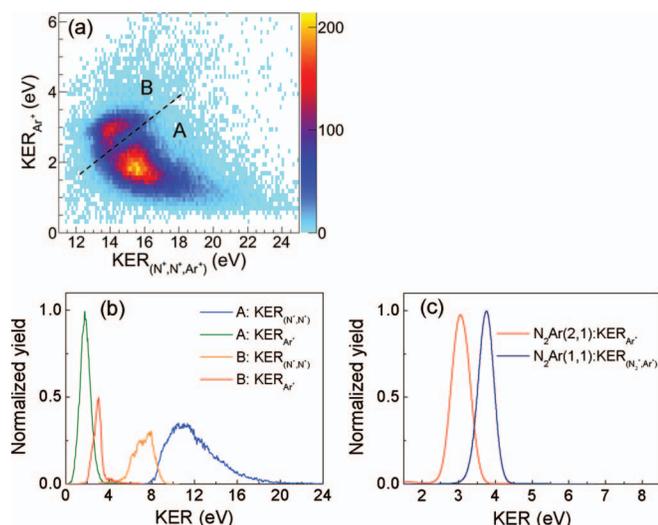
FIG. 1. (a) Density plot of KER_{Ar+} vs $KER_{(N+,N+,Ar+)}$ of the triple-ionization-induced three-body breakup channel $N_2Ar(1,1,1)$. (b) KER_{Ar+} and $KER_{(N+,N+)}$ for events in regions A and B as labeled in (a). (c) KER of the double ionization channel $N_2Ar(1,1)$ and KER_{Ar+} from the triple ionization channel $N_2Ar(2,1)$.
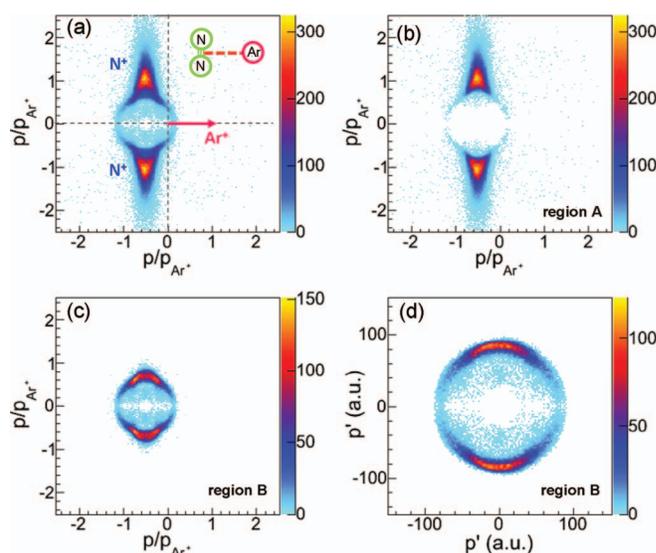

FIG. 2. Newton plots of the triple-ionization-induced three-body breakup channel $N_2Ar(1,1,1)$ for (a) all events, (b) events in region A, and (c) events in region B as labeled in Fig. 1(a). In (a)-(c) the momenta are normalized to the momentum of the Ar^+. (d) The same as (c) but without momentum vector normalization and the recoil of the Ar^+ is subtracted from the momenta. The inset of (a) illustrates the T-shaped structure of the N_2Ar dimer.

three particles is larger than 11 eV so that all the particles are from the three-body breakup. This reliably sorts out the background from the exploding double ionization of the diatomic molecule and single ionization of the atomic monomer in the same pulse.

Figure 1(a) shows the KER of Ar^+, i.e., KER_{Ar+} = $0.5|p_{Ar+}|^2/m_{Ar}$, versus the total KER, i.e., $KER_{(N+,N+,Ar+)}$ = $KER_{N+} + KER_{N+} + KER_{Ar+}$, of the three-body breakup $N_2Ar^{3+} \rightarrow N^+ + N^+ + Ar^+$. We refer to this channel as $N_2Ar(1,1,1)$ below. Note that the KER of Ar^+ is less than 20% of the total [see Fig. 1(a)]. This directly reflects that the N_2–Ar van der Vaals bond is much longer than the N–N covalent bond. The corresponding Newton diagram of $N_2Ar(1,1,1)$ channel is shown in Fig. 2(a). The momentum vector of Ar^+ is represented by a red arrow fixed at unity pointing to the right, and the momentum vectors of two coincident N^+ from the same dimer are normalized to the length of Ar^+ and mapped to the left side. It reveals a T-shaped structure of N_2Ar as illustrated by the inset of Fig. 2(a) in agreement with the spectroscopy measurements[1,2] and theoretical calculations.[3–5]

As labeled with A and B in Fig. 1(a), there are two regions of the KER distribution, indicating either two different ionization dynamics or structures of the N_2Ar dimer. To get into the details, we plot the corresponding Newton diagrams in Figs. 2(b) and 2(c). For region A, the concentrated distribution of N^+ [Fig. 2(b)] indicates that it is from direct three-body breakup of triply ionized T-shaped N_2Ar dimer. For region B, the N^+ is mostly distributed on the ring [Fig. 2(c)]. There are two possible reasons to form this ring-like structure: (a) the N_2^{2+} can rotate before fragmenting, so that the breakup axis of the N_2^{2+} get randomized and does not correspond to the internal N_2 axis, as observed in the fragmentation of CO_2[15] or (b) it could indicate a non-T-shaped initial structure. Our measured KER correlations shown in Fig. 1(a) allow excluding scenario (b). Classical dynamics simulations show that any structure differing from the T-shaped one will increase both KER_{Ar+} and $KER_{(N+,N+,Ar+)}$

as compared to the direct breakup of a T-shaped N_2Ar^{3+}. Such non-T-shaped structures if they result in the observed larger total KER would be located to the upper right of structure A in Fig. 1(a), while our observed structure B is located to the up left of structure A. This indicates a sequential breakup for events in region B. After single ionization on Ar site and double ionization on N_2 site, the dimer ion starts to dissociate along the potential curve of $N_2^{2+} + Ar^+$; The N_2^{2+} rotates when it is departing from Ar^+ and lately breaks into $N^+ + N^+$, which yields a board distribution of N^+ on the ring as shown in Fig. 2(c) [or Fig. 2(d) without momentum vector normalization].

This sequential three-body breakup scenario is corroborated by the distributions of the KER_{Ar+} and the KER of $N^+ + N^+$ pair, $KER_{(N+,N+)} = |p_{rel(N+,N+)}|^2/m_N$, where $p_{rel(N+,N+)}$ is the relative momentum between two mutually repelling N^+. The KER_{Ar+} from the sequential three-body breakup [region B, Fig. 1(b)] is very similar to that from the two-body breakup $N_2Ar^{3+} \rightarrow N_2^{2+} + Ar^+$ channel [Fig. 1(c)], referred as $N_2Ar(2,1)$, since it is the intermediate state. Meanwhile, due to the population of the bound sates of N_2^{2+} following the double ionization of the N_2 site, the $KER_{(N+,N+)}$ from the sequential three-body breakup shows several fine structures [Fig. 1(b)]. They correspond to vibrational modes of the intermediate metastable N_2^{2+}[27] which dissociates with delay by coupling to a repulsive curve. For direct three-body breakup in region A, as shown in Fig. 1(b), both KER_{Ar+} and $KER_{(N+,N+)}$ distributions are different as compared to the sequential one in region B. Therefore, N_2Ar features a T-shaped structure,[1–5] where the bond axis of N_2 is perpendicular to the dimer axis as illustrated by the inset of Fig. 2(a). It undergoes direct or sequential three-body breakup following triple ionization by our intense laser pulse.

For van der Waals-bound dimers composed of heavy nuclei, the ultrashort laser pulse driven Coulomb explosion is

known to nicely map the equilibrium distance in the ground state nuclear wavefunction to the KER distribution of the fragment ions.[21,28] Also for the mixed systems studied here, the Ar and N_2 in N_2Ar dimer are frozen during the ultrafast ionization process, which subsequently explode due to the strong Coulomb repulsion between the multiply charged ions. The equilibrium distance between Ar and the center-of-mass of N_2 at the instant of multiple ionization can be classically approximated to $R_{N2-Ar} \sim q_1 q_2 / KER_{(N2q1+, Arq2+)}$, where $KER_{(N2q1+, Arq2+)}$ is the KER of the exploding channel $N_2Ar^{(q1+q2)+} \rightarrow N_2^{q1+} + Ar^{q2+}$. For $KER_{(N2+, Ar+)} \sim 3.7$ eV of the two-sites double ionization channel $N_2Ar(1,1)$ measured in our experiment as shown in Fig. 1(c), we calculate $R_{N2-Ar} \sim 3.86$ Å for N_2Ar. This imaging of the bond length does not work for the internal N_2 bond for two reasons. Firstly, due to the enhanced multiple ionization[29,30] of the light diatomic molecule at a critical internuclear distance, our 35-fs laser pulse is not short enough and secondly, the N^+–N^+ potential strongly depends on the electronic state and is not necessary being $1/R$. For the direct three-body breakup channel $N_2Ar(1,1,1)$ in region A, as shown in Fig. 1(b), $KER_{(N+, N+)}$ shows a broad distribution with a maximum around ~ 11 eV. For a $1/R$ potential, this would correspond to a double ionization of N_2 inside N_2Ar at $R_{N-N} \sim 1.32$ Å.

Similar to N_2Ar, as shown in Fig. 3(a), O_2Ar also shows a T-shaped structure,[7,8] where the bond of O_2 is perpendicular to the dimer axis as illustrated by the inset. Figure 4(a) shows the KER distribution of Ar^+ as a function of the total KER, i.e., $KER_{(O+, O+, Ar+)} = KER_{O+} + KER_{O+} + KER_{Ar+}$, of the three-body breakup channel $O_2Ar^{3+} \rightarrow O^+ + O^+ + Ar^+$ which is referred as $O_2Ar(1,1,1)$. It shows two regions C and D. The main distribution of region C represents the direct three-body breakup of the T-shaped O_2Ar as visu-

FIG. 4. (a) Density plot of KER_{Ar+} vs $KER_{(O+, O+, Ar+)}$ of the triple-ionization-induced three-body breakup channel $O_2Ar(1,1,1)$. (b) KER of the double ionization channels $O_2Ar(1,1)$ and $O_2Xe(1,1)$, and $KER_{(O+, O+)}$ from $O_2Ar(1,1,1)$ channel.

alized by the Newton diagram in Fig. 3(b). The location of the counts in region D is very different from region B in the N_2Ar case [Fig. 1(a)]. The counts in region D is displaced to the upper right of the maximum in region C, i.e., a high KER of the Ar^+ goes along with an increase of the total KER. As we have argued above this indicates that these events are from a direct breakup of a somewhat more linear structure than the T-shape. The Newton diagram in Fig. 3(c) visualizes the details, where O^+ are found preferentially on four spots on a ring. Figure 3(d) shows the same data as Fig. 3(c) but without normalization of the momentum vectors. This excludes that the distribution is an artifact caused by the normalization. We therefore conclude that the four spots structure originates from direct Coulomb explosion from a structure of the O_2Ar which is different from the dominating T-shaped one.

This structural difference between the purely T-shaped N_2Ar, the additional structure of O_2Ar, likely originates from the different shape of the highest occupied molecular orbital (HOMO) of O_2 compared to N_2. For N_2, the HOMO with σ_g symmetry[31] concentrates around the nuclei along the molecular axis. For O_2, the HOMO with π_g symmetry[31] features butterfly shaped four lobes with a node along the molecular axis. As compared to N_2Ar with its stable T-shaped geometry, one might expect O_2Ar to have additional structures where the dimer potential finds its local minimums.

The equilibrium distance between Ar and the center-of-mass of O_2 in O_2Ar is estimated to be $R_{O2-Ar} \sim 3.65$ Å based on the measured $KER_{(O2+, Ar+)} \sim 3.9$ eV of the double ionization channel $O_2Ar(1,1)$ as shown in Fig. 4(b). For the
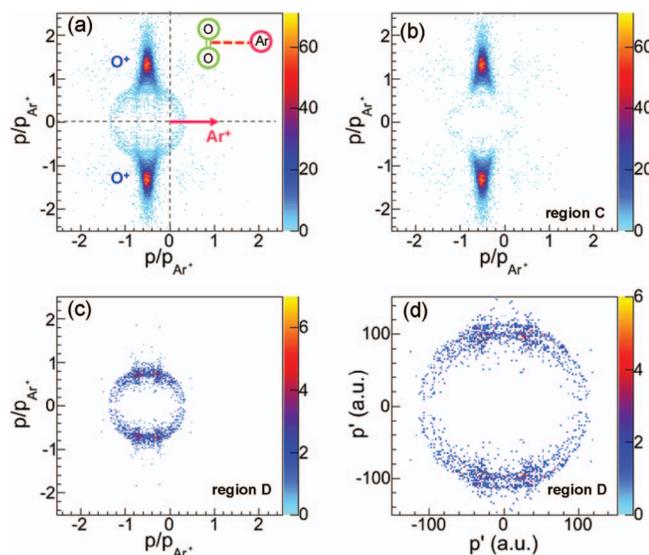

FIG. 3. Newton plots of the triple-ionization-induced three-body breakup channel $O_2Ar(1,1,1)$ for (a) all events, (b) events in region C, and (c) events in region D as labeled in Fig. 4(a). In (a)-(c) the momenta are normalized to the momentum of the Ar^+. (d) The same as (c) but without momentum vector normalization and the recoil of the Ar^+ is subtracted from the momenta. The inset of (a) illustrates the T-shaped structure of the O_2Ar dimer.
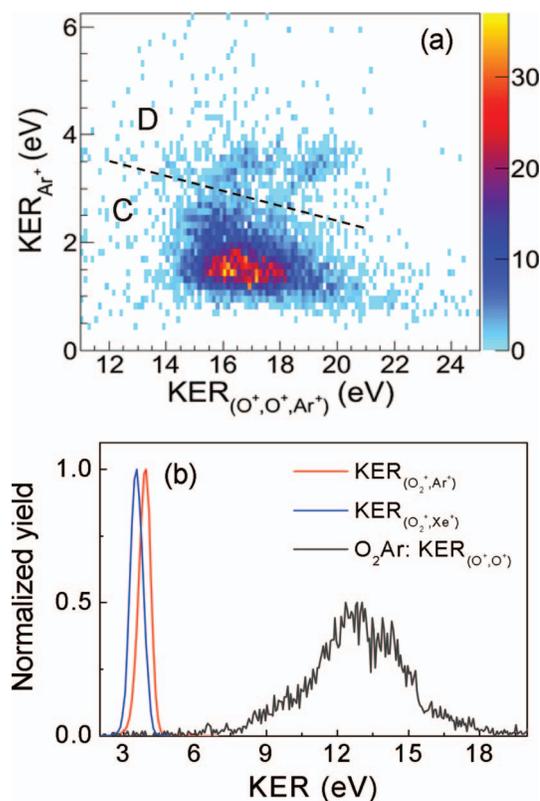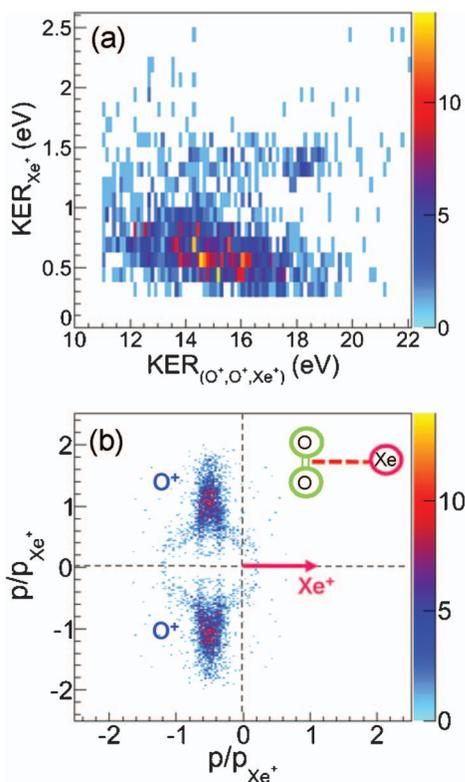
FIG. 5. (a) Density plot of KER_{Xe+} vs $KER_{(O+,O+,Xe+)}$ of $O_2Xe(1,1,1)$ channel. (b) Newton plot of the triple-ionization-induced three-body breakup channel $O_2Xe(1,1,1)$. The momenta are normalized to the momentum of the Xe^+. The inset illustrates the T-shaped structure of O_2Xe.

$O^+ + O^+$ pair in the three-body breakup $O_2Ar(1,1,1)$ channel, a broad distribution of $KER_{(O+,O+)}$ is observed around ~ 12.8 eV [see Fig. 4(b)]. Assuming an (unrealistic) $1/R$ potential for the $O^+ - O^+$ this would correspond to $R_{O-O} \sim 1.11$ Å.

For O_2Xe, there are seven Xe isotopes that can contribute to form the dimer with O_2 in our jet. All the isotopes are found to have similar structure and ionization dynamics. Figure 5(a) displays the distribution of KER_{Xe+} as a function of $KER_{(O+,O+,Xe+)}$ for the triple-ionization-induced three-body breakup channel $O_2Xe^{3+} \rightarrow O^+ + O^+ + Xe^+$, referred as $O_2Xe(1,1,1)$. The corresponding Newton diagram is shown in Fig. 5(b). They are very similar to those of $O_2Ar(1,1,1)$ as shown in Figs. 3(a) and 4(a), indicating same structures and ionization dynamics. For $KER_{(O2+,Xe+)} \sim 3.5$ eV of the double ionization channel $O_2Xe(1,1)$ as shown in Fig. 4(b), we estimate the equilibrium distance between Xe and the center-of-mass of O_2 in O_2Xe is $R_{O2-Xe} \sim 4.07$ Å.

In summary, by using intense ultrashort laser pulse to multiply ionize and Coulomb explode the molecule-atom dimers, we directly map their equilibrium geometries to the detected momenta of the fragment ions. All the molecule-atom dimers investigated in this work, i.e., N_2Ar, O_2Ar, and O_2Xe, are observed to have a T-shaped structure[1–5,7,8,10–12] in which the bond of the contained diatomic molecule is perpendicular to the dimer axis. For O_2Ar and O_2Xe, different structures are observed to coexist with the dominating T-shaped one. This difference between N_2 contained dimer and the one with O_2 might be related to the difference between HOMOs of

N_2 and O_2 molecules. The equilibrium distance between the rare-gas atom and the center-of-mass of the molecule is estimated to be $R_{N2-Ar} \sim 3.86$ Å, $R_{O2-Ar} \sim 3.65$ Å, and $R_{O2-Xe} \sim 4.07$ Å, respectively, for N_2Ar, O_2Ar, and O_2Xe.

[1] G. Henderson and G. E. Ewing, Mol. Phys. **27**, 903 (1974).
[2] W. Jäiger and M. C. L. Gerry, Chem. Phys. Lett. **196**, 274 (1992).
[3] K. Patel, P. R. Butler, A. M. Ellis, and M. D. Wheeler, J. Chem. Phys. **119**, 909 (2003).
[4] C. R. Munteanu, J. L. Cacheiro, and B. Fernández, J. Chem. Phys. **121**, 10419 (2004).
[5] J. Zhu, Y.-P. Lu, X.-R. Chen, and Y. Cheng, Eur. Phys. J. D **33**, 43 (2005).
[6] F. Wang, F. R. W. McCourt, and R. J. Le Roy, J. Chem. Phys. **113**, 98 (2000).
[7] G. Henderson and G. E. Ewing, J. Chem. Phys. **59**, 2280 (1973).
[8] J. Mettes, B. Heymen, P. Verhoeve, J. Reuss, D. C. Lainé, and G. Brocks, Chem. Phys. **92**, 9 (1985).
[9] F. A. Gianturco and A. Storozhev, J. Chem. Phys. **101**, 9624 (1994).
[10] V. Aquilanti, D. Ascenzi, D. Cappelletti, M. de Castro, and F. Pirani, J. Chem. Phys. **109**, 3898 (1998).
[11] A. V. Baklanov, G. A. Bogdanchikov, K. V. Vidma, D. A. Chestakov, and D. H. Parker, J. Chem. Phys. **126**, 124316 (2007).
[12] K. V. Vidma, G. A. Bogdanchikov, A. V. Baklanov, D. A. Chestakov, and D. H. Parker, J. Chem. Phys. **133**, 194306 (2010).
[13] Z. Vager, R. Naaman, and E. P. Kanter, Science **244**, 426 (1989).
[14] N. Neumann, D. Hant, L. Ph. H. Schmidt, J. Titze, T. Jahnke, A. Czasch, M. S. Schöffler, K. Kreidi, O. Jagutzki, H. Schmidt-Böcking, and R. Dörner, Phys. Rev. Lett. **104**, 103201 (2010).
[15] Y. Muramatsu, K. Ueda, N. Saito, H. Chiba, M. Lavollée, A. Czasch, T. Weber, O. Jagutzki, H. Schmidt-Böcking, R. Moshammer, U. Becker, K. Kubozuka, and I. Koyano, Phys. Rev. Lett. **88**, 133002 (2002).
[16] F. Légaré, K. F. Lee, I. V. Litvinyuk, P. W. Dooley, S. S. Wesolowski, P. R. Bunker, P. Dombi, F. Krausz, A. D. Bandrauk, D. M. Villeneuve, and P. B. Corkum, Phys. Rev. A **71**, 013415 (2005).
[17] K. Zhao and W. T. Hill III, Phys. Rev. A **71**, 013412 (2005).
[18] J. Gagnon, K. F Lee, D. M. Rayner, P. B. Corkum, and V. R. Bhardwaj, J. Phys. B **41**, 215104 (2008).
[19] A. Hishikawa, H. Hasegawa, and K. Yamanouchi, Chem. Phys. Lett. **388**, 1 (2004).
[20] J. P. Brichta, S. J. Walker, R. Helsten, and J. H. Sanderson, J. Phys. B **40**, 117 (2007).
[21] B. Ulrich, A. Vredenborg, A. Malakzadeh, L. Ph. H. Schmidt, T. Havermeier, M. Meckel, K. Cole, M. Smolarski, Z. Chang, T. Jahnke, and R. Dörner, J. Phys. Chem. A **115**, 6936 (2011).
[22] L. Ph. H. Schmidt, T. Jahnke, A. Czasch, M. Schöffler, H. Schmidt-Böcking, and R. Dörner, Phys. Rev. Lett. **108**, 073202 (2012).
[23] J. Ullrich, R. Moshammer, R. Dörner, O. Jagutzki, V. Mergel, H. Schmidt-Böcking, and L. Spielberger, J. Phys. B **30**, 2917 (1997).
[24] R. Dörner, V. Mergel, O. Jagutzki, L. Spielberger, J. Ullrich, R. Moshammer, and H. Schmidt-Böcking, Phys. Rep. **330**, 95 (2000).
[25] A. S. Alnaser, X. M. Tong, T. Osipov, S. Voss, C. M. Maharjan, B. Shan, Z. Chang, and C. L. Cocke, Phys. Rev. A **70**, 023413 (2004).
[26] O. Jagutzki, V. Mergel, K. Ullmann-Pfleger, L. Spielberger, U. Spillmann, R. Dörner, and H. Schmidt-Böcking, Nucl. Instrum. Methods Phys. Res. A **477**, 244 (2002).
[27] N. A. Cherepkov, S. K. Semenov, M. S. Schöffler, J. Titze, N. Petridis, T. Jahnke, K. Cole, L. Ph. H. Schmidt, A. Czasch, D. Akoury, O. Jagutzki, J. B. Williams, C. L. Cocke, T. Osipov, S. Lee, M. H. Prior, A. Belkacem, A. L. Landers, H. Schmidt-Böcking, Th. Weber, and R. Dörner, Phys. Rev. A **80**, 051404(R) (2009).
[28] J. Wu, A. Vredenborg, B. Ulrich, L. Ph. H. Schmidt, M. Meckel, S. Voss, H. Sann, H. Kim, T. Jahnke, and R. Dörner, Phys. Rev. Lett. **107**, 043003 (2011).
[29] T. Seideman, M. Yu. Ivanov, and P. B. Corkum, Phys. Rev. Lett. **75**, 2819 (1995).
[30] S. Chelkowski and A. D. Bandrauk, J. Phys. B **28**, L723 (1995).
[31] S. Petretti, Y. V. Vanne, A. Saenz, A. Castro, and P. Decleva, Phys. Rev. Lett. **104**, 223001 (2010).